Available online at www.sciencedirect.com
SCIENCE DIRECT®
ELSEVIER
Earth and Planetary Science Letters 6931 (2003) 1–20
EPSL
www.elsevier.com/locate/epsl

# Thermo-mechanical controls on the mode of continental collision in the SE Carpathians (Romania)

S.A.P.L. Cloetingh [a,*], E. Burov [b], L. Matenco [a], G. Toussaint [b], G. Bertotti [a], P.A.M. Andriessen [a], M.J.R. Wortel [c], W. Spakman [c]

[a] *Netherlands Centre for Integrated Solid Earth Sciences, Vrije Universiteit, Faculty of Earth and Life Sciences, De Boelelaan 1085, 1081 HV Amsterdam, The Netherlands*

[b] *Université Pierre et Marie Curie, Laboratoire de Tectonique, 4 Place Jussieu, 75252 Paris Cedex 05, France*

[c] *Netherlands Centre for Integrated Solid Earth Sciences, Universiteit Utrecht, Faculty of Earth Sciences, P.O. Box 80.021, 3508 TA Utrecht, The Netherlands*

Received 22 August 2003; received in revised form 3 November 2003; accepted 7 November 2003

**Abstract**

The Carpathians orogenic system, with its along-arc variations in topography developed in the aftermath of continental collision, is associated with unusual foredeep basins, large-scale strain and seismicity concentration and high-velocity mantle bodies. The East Carpathians continental collision was non-cylindrical, leading to large-scale variations in thrust nappe kinematics, orogenic uplift patterns and foredeep subsidence, controlled by the mechanics and geometry of the lower plate. Thermo-mechanical modelling demonstrates that in this low-rate convergence regime, the subducted lithosphere had enough time to interact with the mantle to advance towards a thermal resettlement. This is favored by the low degree of metamorphism, mechanical weakness of the lower plate and the lack of active surface processes at the contact with and in the upper plate. In contrast, low-buoyant, thick lower crust and active surface processes keep the continuity of the slab intact and promote the development of typical foredeep basins. The model explains in a self-consistent manner the unusual geometry of the Vrancea seismogenic slab in the bend zone of the Romanian Carpathians. The model is also consistent with the presence of two high-velocity bodies inferred from seismic tomography studies and explains the depth zonation of seismicity in the Vrancea area. Differences between the northern part of East Carpathians and the southeastern bend of the Carpathians arc are largely controlled by lateral variations in crustal structure, topography emplacement and surface processes along the arc. Mechanical heterogeneity of the Carpathians subduction leads to the development of two end member modes of collision, allowing a study of these states and their transition. Lithospheric configuration and tectonic topography appear to be prime factors controlling variations in slab behavior. In the SE Carpathians, at the terminal phase of continental convergence, slab delamination, roll-back and depocenter migration appear to play a more limited role at shallow and lithospheric levels.


* Corresponding author: Fax: +31-20-4449943.
*E-mail addresses:* sierd.cloetingh@falw.vu.nl (S.A.P.L. Cloetingh), evgenii.burov@lgs.jussieu.fr (E. Burov), liviu.matenco@falw.vu.nl (L. Matenco), gisele.toussaint@lgs.jussieu.fr (G. Toussaint), giovanni.bertotti@falw.vu.nl (G. Bertotti), paul.andriessen@falw.vu.nl (P.A.M. Andriessen), wortel@geo.uu.nl (M.J.R. Wortel), wims@geo.uu.nl (W. Spakman).

0012-821X/03/$ – see front matter © 2003 Published by Elsevier B.V.
doi:10.1016/S0012-821X(03)00645-9

*Keywords:* continental collision; tectonic topography; thermo-mechanical modelling; unstable subduction; Carpathians

## 1. Introduction

The Carpathians orogenic system has a spatially varied along-arc tectonic topography developed in the aftermath of continental collision. It represents a natural example for the study of unusually developed foredeep basins associated with large-scale strain and seismicity concentration and high-velocity mantle bodies. Over the last few years, attention has been focused on spatial and temporal variations in thrusting along the Carpathians arc and their relationship to unusual foredeep geometry and lateral variations in flexural behavior. The reconstruction of uplift and erosion history in and around the Carpathians (e.g. [1]), coupled with subsidence modelling in its foreland [2], have elucidated the complex interplay of flexural downloading during collision, followed by unroofing linked to unflexure and isostatic rebound [3,4].

The timing of Carpathians continental collision reflects the stage when non-thinned lower plate starts to underplate during convergence. This collision has been demonstrated to be a non-cylindri-

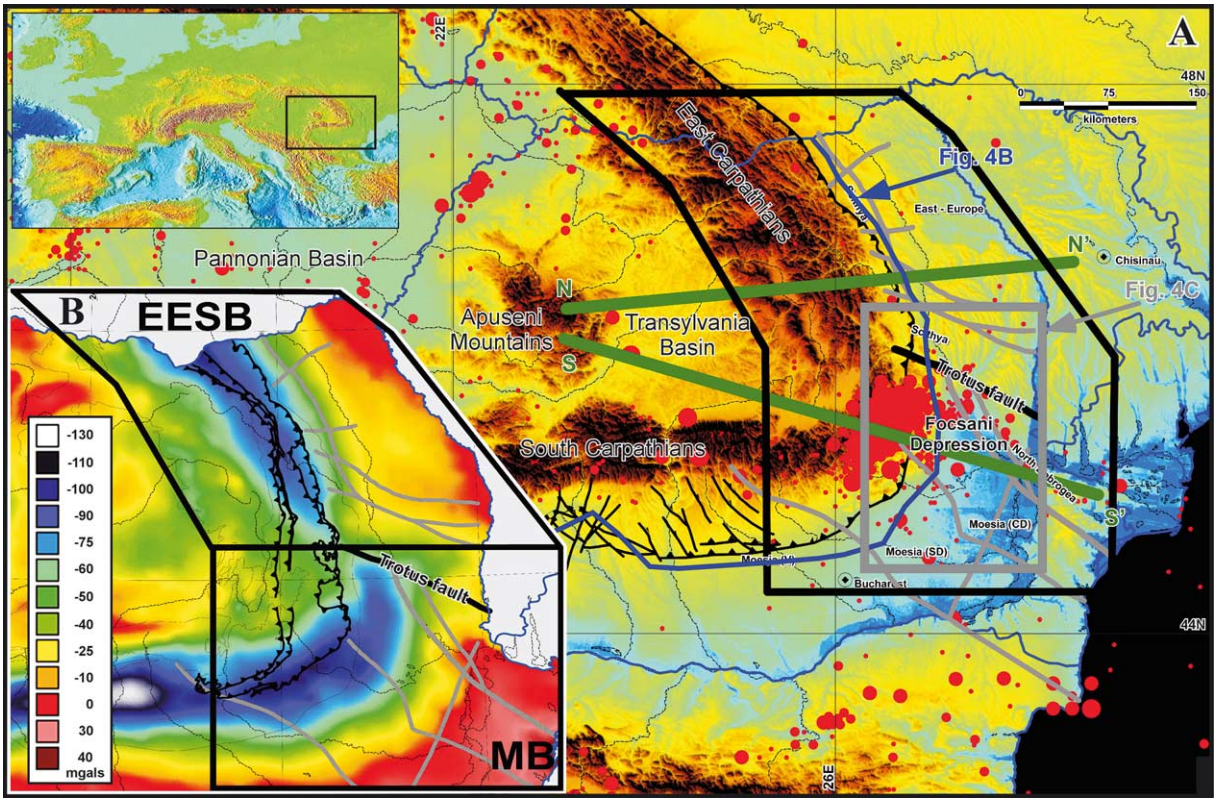


Fig. 1. (A) Topographic map of the Romanian Carpathians with the location of modelled cross-sections (N-N′ and S-S′). Note the clustering of earthquakes (red dots) in the Vrancea seismic area in the bend zone of the Carpathians arc and the topographic difference between the East European/Scythian–North Dobrogean (EESB) and the Moesian domains (MB). Black and gray lines mark location of major crustal scale fault zones (see Fig. 4 for further details). (B) Bouguer gravity map of Romania, anomalies in mgal (after [8]). Black boxes mark the areas affected by the collision with the EESB and MB which are characterized by differences in thermo-mechanical age of the underthrusted lithosphere, coinciding with the offset in the gravity anomaly at the location of the crustal-scale Trotus fault (TF).

cal process, leading to strong deviations from 2D strain geometries. This is associated with large-scale variations in thrust nappe kinematics, orogenic uplift patterns and foredeep subsidence, in relation to the mechanics and geometry of the lower plate [2,5]. As for most other collision orogens, the Carpathians continental collision takes place at significantly lower rates than oceanic subduction, due to the buoyancy of the continental crust involved in subduction/underthrusting. Upper continental crust cannot be involved directly in subduction and convergence can continue only when it is decoupled/delaminated from the mantle or transformed into higher-density materials (e.g. [6]). As a result of low convergence rates, the subducted lithosphere has enough time to interact with the mantle and to advance towards thermal re-equilibration. This latter process is enhanced [7] by low degrees of metamorphism, a mechanically weak lower plate and by gentle topography and lack of active surface processes at the contact with and in the upper plate. In contrast, dense, thick lower crust, coupled with high topography/active surface processes keeps the slab intact and facilitates the development of typical foredeep basins.

In this paper we show that the contrasting character of the underthrusted East European/Scythian (EESB) and the Moesian (MB) blocks could have played a significant role in the subduction mechanism and the associated development of overlying foredeep basins (Fig. 1A). The contrast in lithosphere geometry is dramatically expressed in the Bouguer gravity anomaly (Fig. 1B), demonstrating a clear offset at the transition between EESB and MB, coinciding with the Trotus fault.

The Carpathians represent one of the birthplace areas of the slab break-off and slab tear migration models, thanks to seismic tomography studies (e.g. [9,10] and references therein) (Fig. 2). Variations of the same model include slab-tearing in various parts of the underthrusted lower plate (e.g. [12]), slab detachment and/or slab delamination (e.g. [13]). All these models assume differences in time and space in the subduction/collision process along the Carpathians arc with, at the scale of the whole orogen, a lower plate acting as a continuous, mechanically constant body at various depths. Collision mechanics in the Carpathians arc also strongly affects extensional basin formation and inversion in the Pannonian domain [14].

### 1.1. Unusual foredeeps and orogenic arc seismicity

One of the most striking features of Carpathians dynamics is the formation and evolution of the Focsani Depression, a 13 km thick Miocene–Pliocene basin (e.g. [15]), situated in the vicinity of the Vrancea earthquake cluster (e.g. [16]) in the southeastern part of the orogenic chain (Fig. 1A). Whether or not this represents the present position of a Benioff plane is disputed, mostly because the peculiar 85° dip of the downgoing lithospheric slab is situated almost in the front of the orogen. This has been so far explained as a late Miocene to Pliocene roll-back effect in the SE Carpathians, which could have culminated when the subducting slab tore (slab detachment sensu [10]) along the trend of the orogenic arc (see [9,12,17] and references therein). The latter is commonly thought to have induced a rebound in the northern, torn, parts of the slab, and subsidence of the lower plate in the bending area, where the slab still holds its integrity: this occurred simultaneously with a fast migration towards the foreland, leading to the opening of the thick foredeep (Focsani) basin. In the SE Carpathians bend zone, deformations along the sole thrust are well dated by Late Miocene to Pliocene sedimentary cover, the final shortening and collisional event having taken place at 11 Ma [18]. Thus younger shortening cannot account for the subsidence migration along orogenic strike (e.g. [18]). Seismic reflection data in the Focsani basin show normal faults associated with subsidence in the middle of the basin and asymmetric rapid Quaternary uplift on each flank. The internal geometry of the basin, recently studied in detail (e.g. [15]), indicates that Miocene to Quaternary sedimentation was roughly symmetrical, in contrast with the wedge-shape pattern characteristic of classical, flexural-controlled foredeep basins. The structure of the crust beneath is similar to the intermediate crustal architecture below Focsani basin [19].

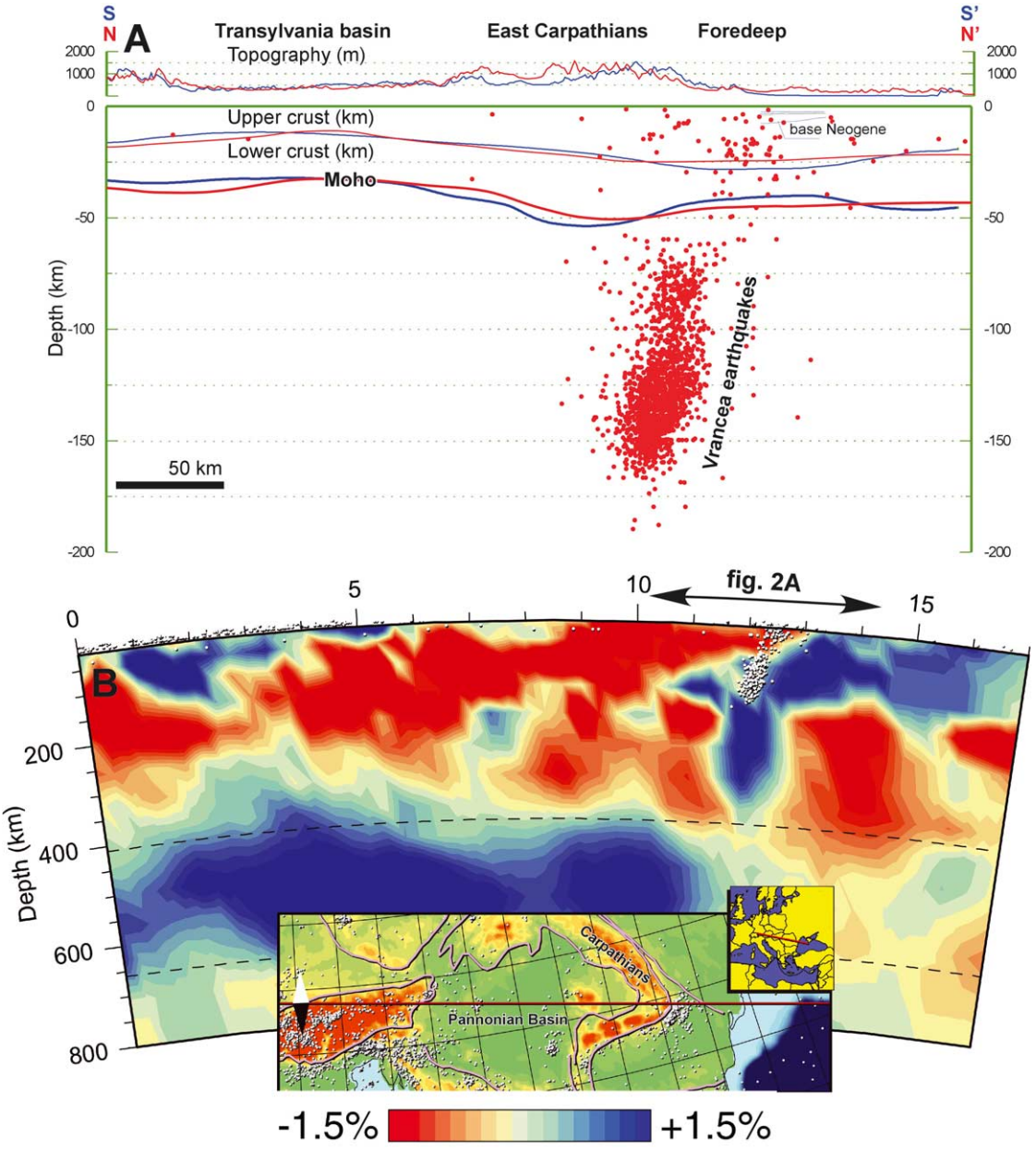


Fig. 2. (A) Crustal-scale cross-sections across the East Carpathians (modified after [11]). Red lines represent the northern cross-section in the area affected by the collision with the East European/Scythian rigid block. Blue lines represent the southern cross-section in the bend area influenced by the collision with highly buoyant Moesian block. Red dots represent earthquake projection into the southern section trace. (B) Seismic tomography (after [10]) across the bend zone of the East Carpathians in the MB domain. Blue and red: positive and negative P-wave anomalies corresponding to the presence of cold and hot mantle in the area, respectively. Open circles give the location of Vrancea earthquakes.

Whereas seismicity is minor in the central–northern segments of the Carpathians chain, the southern part of the belt is the site of the largest strain accumulation in Europe [9]. The high earthquake recurrences (10 years for $M_w > 6.5$, 25 years for $M_w > 7$, and 50 years for $M_w > 7.4$) are limited to a spatially restricted, $40 \times 80 \times 200$ km, seismogenic volume [16], laterally shifted towards the southeast by $\sim 100$ km with respect to the expected position of the plate boundary in a typical geometry of a collision system (Fig. 2). High-resolution local seismic tomography studies [20] have demonstrated the presence of two high-velocity bodies in the SE Carpathians. This internal geometry of the high-velocity structure of the Vrancea slab confirms previous inferences from regional tomography (e.g. [10,21]). The Vrancea earthquakes cluster mostly within the first, northeastern high-velocity body. The second one, further southeast, has no significant seismicity signature, being apparently separated from the first, at least at crustal levels. In addition, the first velocity body appears to contain zones of thinning distributed vertically [20].

### 1.2. Lateral variations in collision mechanics

The main collisional event was coherent and simultaneous along the entire chain at approx. 11 Ma (e.g. [18]), but its mechanics and effects are different in the two sectors of the chain (Fig. 3A). Collision in the central–northern domain was controlled by the dense EESB, a cold cratonic lithosphere with a thermo-mechanical age of at least 150–200 Ma: this corresponds to a strong mantle lid and large lithosphere bulk strength (see [22]). This block has a thick crust below syn- and post-collisional sediments and a typical, 3–6 km wedge-shaped foredeep. As a result of the stable indentation, up to 5 km of uplift and sub-

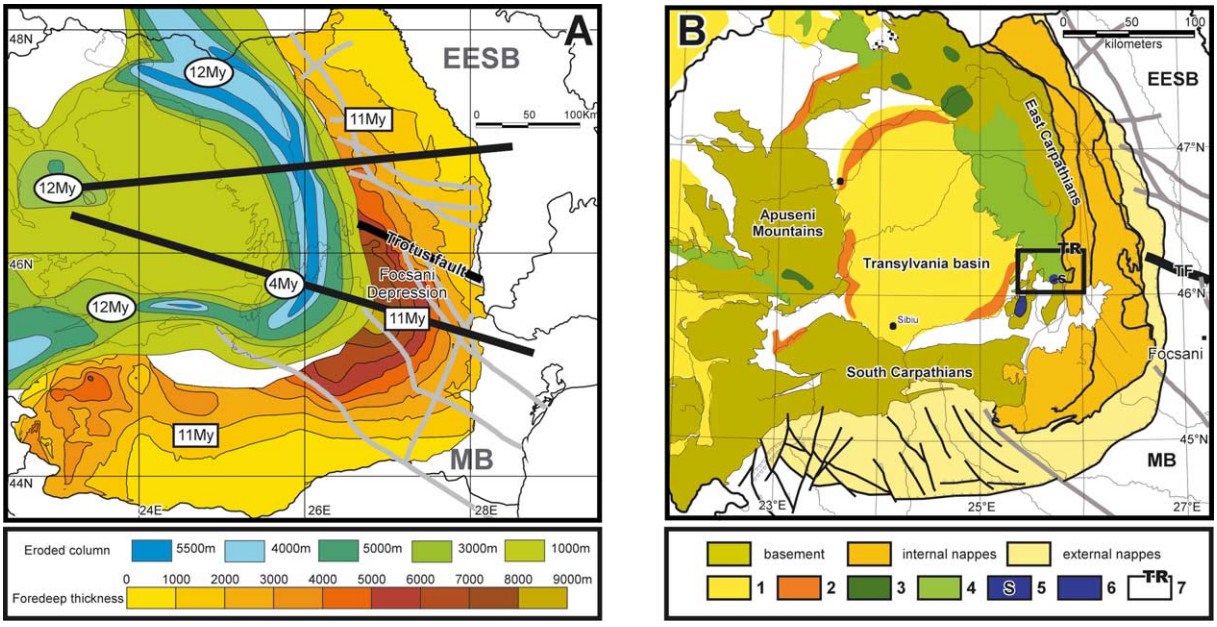


Fig. 3. (A) Spatial variations in uplift and erosion along the Romanian Carpathians inferred from geothermochronology studies (after [1]) and thickness of foredeep sediments in the Romanian Carpathians foreland. Elliptical boxes indicate the time of uplift in the upper plate, while square boxes indicate the main moment of subsidence. Note the pronounced lateral differences in uplift ages along the arc, while the main subsidence period is coeval along the studied area. (B) Location and distribution of Neogene–Quaternary igneous rocks in the Romanian Carpathians backarc zone (modified from [36]). 1, 2: pre-collision acidic calc-alkaline volcanism (1: buried, 2: outcropping), 3, 4: syn- and post-collision intermediate calc-alkaline magmatism (3: intrusive outcropping, 4: stratovolcanic outcropping), 5: shoshonitic magmatism, 6: alkali-basaltic volcanism, 7: transition area from calc-alkaline to alkali-basaltic magmatism.

sequent erosion took place during the collision [1], pre-dating minor deformation and sedimentation in the Pliocene–Quaternary (Fig. 3A).

In contrast, collision in the southern domain was controlled by the highly buoyant MB foreland, which was affected by recent (14–15 Ma) extensional re-heating of the lithosphere [15], leading to a considerable reduction of its bulk strength. This block has a thin crust below thick syn- and post-collisional sediments. 2–4 km of largely post-collision (4–0 Ma) uplift and erosion was coeval with deformation and sedimentation of up to 9 km syn- and post-collision deposits (Fig. 3A).

Thermal modelling of the collision process in the East Carpathians (e.g. [23]) indicates that oceanic subduction during continental pre-collision has also important effects on the thermal and rheological structure of the lithosphere. Rheological modelling [23,24] demonstrates that crustal and mantle deformation, associated with the deep earthquake zone in the area dominated by the MB, are decoupled.

Below we will argue that the nature of the lithosphere involved in the East Carpathians collision plays a key role in the relationship between sedimentary basin formation, deep lithospheric processes and near-surface deformation. Quantitative analysis of bulk rheology, *P–T–t* data and thermo-mechanical modelling provide essential constraints on both the loading evolution of the thin-skinned belt and the analysis of local kinematic deformation.

We will demonstrate that, although complex, the Carpathians tectonic setting with mechanically heterogeneous subducting/underthrusting plates provides an opportunity to study in detail end member modes of collision and transition between these states.

## 2. Geological and geophysical data

New constraints have become available recently on the timing and magnitude of strain localization and vertical motions along the Carpathians arc. In particular, a large database has been developed for the Miocene to Recent (see [25,26]).

### 2.1. Timing of continental collision

The Alpine tectonic evolution of the Carpathians can be divided into a Triassic to Early Cretaceous phase of extension followed by Middle Cretaceous to Miocene shortening (e.g. [18,27] and references therein). The Carpathians consist of a nappe pile of crystalline rocks with a Late Paleozoic to Mesozoic sedimentary cover and, in an external position, an Early Cretaceous to Tertiary thin-skinned belt. The present contact between the upper Carpathians nappe pile and the lower continental plate is situated in the 'outer-Dacidian trough', a thinned continental [27] to supposedly oceanic embayment (e.g. [17] and references therein) developed at the contact between the Rhodopian fragment (sensu [28]) and the stable European to Moesian foreland. A large retreating subduction zone was defined at the boundary between the East Carpathians foreland platforms and the orogenic belt [29]. Interpretations like that of Csontos [30] (see also [17,31,32]) assume that the upper plate kinematics is the effect of clockwise rotation of a small continental block (Tisza–Dacia) in the southern part of the Carpathian chain, around the Moesian promontory. During Paleogene–Early Miocene times, this rotation caused NNE–SSW to ENE–WSW shortening in the internal Moldavides nappes. Middle Miocene (Badenian and Sarmatian, 16–10 Ma) deformations led to E–W shortening [18], possibly driven by the roll-back suction of the lower plate [29]. Though all the Miocene events supposedly underthrust continental (thinned) crust [27], the younger, Sarmatian, deformation represents the principal stage of continental collision, marking the onset of Carpathians thrusting over the stable non-thinned platform-type foreland. Later Pliocene to Quaternary NW–SE (to N–S) shortening in the East Carpathians led only to small-scale out-of-sequence deformation, mainly concentrated in the external parts of the junction zone between the East and South Carpathians. In the foreland units of the Carpathians bend area Pliocene to Recent deformation was widespread, with major subsidence in the Focsani basin depocenter and rapid flank uplift (e.g. [33]). While the large-scale shortening took place during the Miocene in

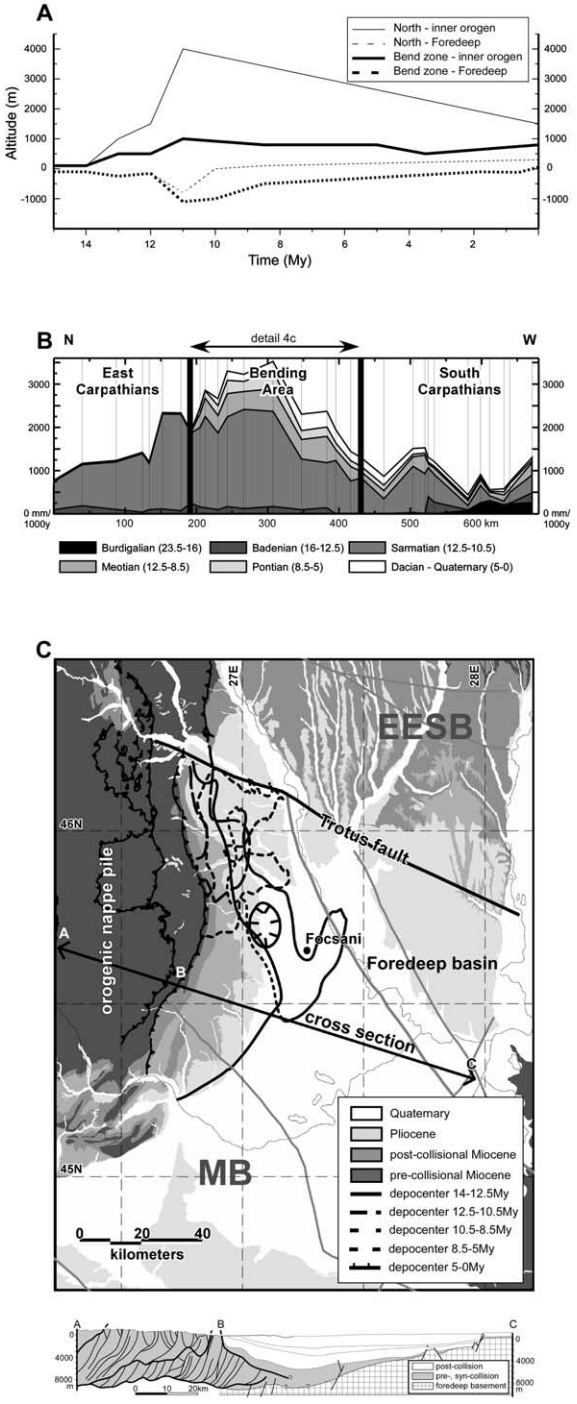


the East Carpathians, accounting for large-scale underthrusting of the lower plate, the low amount of contraction in the South Carpathians, west of the bend zone (e.g. [32]), disables subduction of the western MB lithosphere in this segment of the Carpathians belt.

In summary, while most of the oceanic/thinned continental subduction took place during the Late Cretaceous to Lower Miocene (e.g. [27]), the main collisional event was coherent and simultaneous along the entire East Carpathians, during the Middle Miocene, at approx. 11 Ma. However, as shown in Section 2.2, its mechanics are completely different in the two sectors of the chain, being controlled by the character of the two lower plate blocks (for a detailed description see [2]).

### 2.2. Constraints on lateral variations along the arc

Collision in the central–northern segment of the belt (Figs. 1A and 2) was characterized by a thick crust, a dense lower plate block, large-scale uplift, active surface processes on the upper plate during collision and high internal shortening at the plate contact. North of the Trotus fault (Fig. 1) the EESB is characterized by a 40–45 km thick crust (20–22 km upper part [34]). The typical wedge-type foredeep developed on top of this block contains 3–6 km of Neogene sediments, developed in front of a highly squeezed nappe pile [18]. Deformation in the lower plate is mainly characterized by coeval thrust faults [15] suggesting mechanical coupling (sensu [35]) with the upper plate deformation. 'Hard' collision induced up to 5 km of

←

Fig. 4. (A) Temporal variations in topography along the two cross-sections selected for thermo-mechanical modelling (compilation after [1,37]). (B) Characteristic subsidence patterns for the lower plate evolution along the segment of the Carpathians arc depicted in Fig. 1. Note that the most important subsidence is coeval in all areas (due to collision). Significant post-collisional subsidence is restricted to the bend area. (C) Map showing the position of syn- and post-collision depocenters along the bend zone of the East Carpathians foredeep and schematic cross-section ABC (bottom) along the external SE Carpathians and the adjacent foredeep. Note the spatial clustering of the depocenters near the Focsani basin and the apparent lack of migration along the orogen.

uplift in the upper plate, initiated at 15–12 Ma (Fig. 3A), during the early stages of convergence [1]. The associated backarc volcanism is calc-alkaline (Fig. 3B). Post-collisional deformation and sedimentation in the orogen and frontal foredeep related to continuation of uplift initiated during the main convergence phase were minor (Fig. 4A). The present-day topography of the foreland is geomorphologically stable at 150–300 m [38].

Collision in the southern segment of the chain (Figs. 1A and 2) was associated with a thin upper crust, a highly buoyant lower plate block, small to negligible uplift, a minor role of surface processes on the upper plate during collision, and low internal shortening at the plate contact. The Moesian lower plate unit in this sector of the belt (Fig. 2) has a crustal thickness of 35–40 km, reaching 40–45 km in the Focsani basin [11,34]. However, the crustal thickness of the block involved in collision is significantly lower, if we take into account the up to 9 km of syn- to post-collisional foredeep sediments (e.g. [2,15]). The sedimentary nappe wedge developed at the plates' contact is characterized by low internal shortening and high offset over the subducting plate. The overall orogenic shortening appears to be lower than elsewhere in the chain. During the main collisional event, no major uplift of the upper plate took place, and consequently no surface processes are recorded by the fission track (FT) studies (e.g. [1]). Uplift and erosion were initiated much later, from 4 Ma onwards, during the post-collisional phase (Figs. 3A and 4A). The associated backarc volcanism is mostly alkaline (Fig. 3B). Deformation in the lower plate is characterized by 14–15 Ma age normal faults in the foreland of the Carpathians bend [15], and smaller-scale extensional structures throughout the Late Miocene to Pliocene. Subsidence in the foredeep remained high in the post-collisional period, leading to the deposition of up to 6 km of Pliocene to Quaternary continental lacustrine-type sediments (Fig. 4B,C). During the Quaternary significant differential vertical motions along and across the arc took place and more than 1 km of sediments accumulated in the foredeep, while a similar amount of uplift is recorded towards the neighboring nappe pile, apparently without thrusting. The entire internal zone is tilted, indicating that differential movements are not controlled by single faults, but are related to large-scale tilting. As a result, topography development along this sector of the foredeep is unequally developed. Quaternary sediments in the western areas are exposed at up to 1000 m elevation, with active erosional patterns, high topographic level terraces, river incisions and braided river systems.

## 3. Modelling

We use the code Parovoz_7 [39], based on the FLAC algorithm [40]. This is a fully coupled thermo-mechanical code that incorporates rheological stratification, brittle–elastic–ductile rheology, surface erosion and metamorphic reactions in the sinking slab (further details in [6,7]). Toussaint et al. [7] recently used this approach to study the dynamics of unstable versus stable slab behavior. The critical parameters of the collision model are density structure, physical and geometrical properties of the upper crust, degree of metamorphism, convergence rate, intensity of surface processes and thermo-tectonic age (geotherm) [7].

### 3.1. Modelling setup

The numerical code uses a moving Lagrangian framework and solves equations of motion (Eq. 1) in large strain mode, coupled with explicit constitutive equations (Eq. 2), thermal transport (Eq. 3) and erosion equations (Eq. 4):

$$\rho\frac{\partial}{\partial t}\left(\frac{\partial \mathbf{u}}{\partial t}\right)-\mathrm{div}\sigma-\rho\mathbf{g}=0 \tag{1}$$

$$\frac{\mathrm{D}\sigma}{\mathrm{D}t}=F\left(\sigma,\mathbf{u},\nabla\frac{\partial \mathbf{u}}{\partial t},\ldots T\ldots\right) \tag{2}$$

$$\frac{\mathrm{D}T}{\mathrm{D}t}=\frac{\partial}{\partial x_i}\left(\chi\frac{\partial T}{\partial x_i}\right)+\frac{H_\mathrm{r}}{\rho C_\mathrm{p}} \tag{3}$$

$$\frac{\partial h}{\partial t}=k_\mathrm{e}\nabla^2 h \tag{4}$$

Here $\rho$, $\mathbf{u}$, $\sigma$, $\mathbf{g}$, $t$, D/D$t$, $F$, $T$, $\chi$, $H_\mathrm{r}$, $C_\mathrm{p}$, $h$, and $k$ are respectively density, velocity vector, stress tensor, acceleration due to gravity vector, time, objective time derivative, functional, temperature,

thermal diffusivity, heat production per unit volume, specific heat, topography and coefficient of erosion. The underlying numerical approach was introduced by Cundall [40] to avoid limitations of implicit finite-element schemes that often have difficulties with treating complex non-linear rheologies. To circumvent these difficulties, the numerical scheme of the code is made explicit in time, which makes it possible to handle complex rheologies. The algorithm uses a finite-difference scheme to solve the governing equations, but, like in many finite-element methods, the grid is formed of constant-strain quadrilateral elements of variable geometry. These elements are composed of four overlapping triangular elements with trilinear shape functions used to derive force balance difference equations for elements in Gaussian formulation.

### 3.1.1. Explicit rheology

The code handles explicit elastic–ductile–plastic non-linear rheology derived from rock mechanics data. In contrast to most mantle-scale models (e.g. [41]), it uses precise techniques more commonly used for small-scale deformation (e.g. [42]). In particular, general equations of motion, rather than Navier–Stokes flow equations, are solved. This code is free of the limitations of fluid dynamics codes that use viscous rheology and only approximately simulate non-viscous behavior through incorporation of pseudo-plastic and pseudo-elastic terms.

### 3.1.2. Full phase changes and strain localization

The algorithm can reproduce brittle and viscous strain localization, which makes it possible to model formation of shear zones and faults. It also takes into account full $P$–$T$–$t$-dependent phase transitions (in this case eclogitization) that affect all material parameters (rheology, density, thermal conductivity).

### 3.1.3. Surface processes

Erosion and sedimentation are incorporated in a straightforward way: the surface elements are truly eroded and re-deposited with appropriate changes in the material phase. Since the erosion rates are equal to 75–90% of the rock uplift rate in actively deforming regions (e.g. [43]), erosion plays a crucial role in orogenic processes. Erosion preferentially removes steepest newly elevated topography (Eq. 4). In case of isostatic compensation of topography, erosion locally discharges the areas of active rock uplift, which provokes additional local isostatic uplift. By doing so erosion thus forces mountain building (of course under condition that the removed material is replaced with new material supplied by tectonic deformation [43], otherwise erosion destroys topography). The surface discharge rate $\mathrm{d}p_e$ associated with erosion is (Eq. 4, Fig. 5A,B):

$$\mathrm{d}p_e = \rho g \frac{\partial h(t,x)}{\partial t} = \rho g k_e \frac{\partial^2 h(t,x)}{\partial x^2} \tag{5}$$

The topography loss tends to be compensated by readjustment of hydrostatic forces acting on the mountain root. Consequently, in simplified case of local isostasy we have:

$$\rho g \frac{\partial h(t,x)}{\partial t} = \Delta\rho g v_i \Rightarrow v_i = \frac{\partial h(t,x)}{\partial t} \frac{\rho}{\Delta\rho} \tag{6}$$

where $\Delta\rho$ is the density contrast between the surface material and the mantle ($\rho/\Delta\rho \approx 4$), $v_i$ is the rate of the compensatory rock uplift at Moho depth. It follows that Moho uplift rate $v_i$ caused by erosion may be about four times faster than the erosion rate itself. In a stable compressional context, far-field tectonic stresses compensate lithostatic pressure; the reduction of the mountain root results in depression, which enables compensatory deformation that restores its initial size and stress balance. This is equivalent to a rigid feedback between the erosion and subsurface uplift rates; in such a system topography grows at the same rate as it is being eroded; acceleration of the erosion rate results in acceleration of the subsurface uplift rate and vice versa [43]. Of course, in more realistic thermo-mechanical settings examined in this study, the coupling between erosion and tectonic processes is less straightforward.

As can be seen, erosion discharge of isostatically compensated surface is equivalent to application of an upward vertical force. For this reason, strong erosion may either prevent the lower plate from subduction or favor an alternative mode of deformation such as folding.

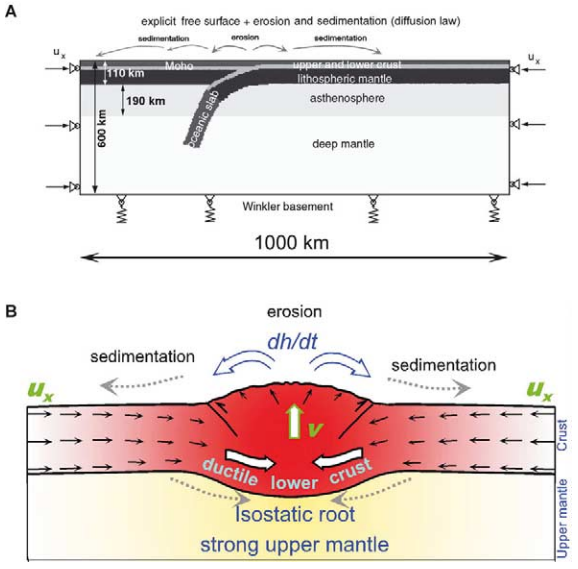


Fig. 5. (A). Thermo-mechanical model setup. The numerical grid is composed of 5×5 km initially rectangular elements. The initial plate geometry corresponds to an already initialized collision. A pre-existing slab of dense oceanic or fully metamorphosed lithosphere is attached at the end of the lower plate to favor subduction at the initial stages of the experiment. Explicit brittle–elastic–ductile rheologies (parameters given in Tables 1 and 2) are used for various lithological zones (shown with different shades of gray). Explicit free surface boundary conditions and surface processes are used at the upper boundary; a Winkler (hydrostatic) boundary condition is used at the base. Lateral boundary conditions are kinematic and are deduced from the data on regional shortening rate (about 60 km/Myr which is equivalent to 15 mm/yr applied at both sides). The initial thermal distribution (computed according to [46,47]), density and rheological structure is specified in Table 2. Density and rheologies are inferred from local seismic, gravity and geological data (see text and Tables 1 and 2). (B) Simplified cartoon explaining interaction between the erosion/sedimentation rate, $\partial h/\partial t$, tectonic shortening rate $u_x$ and vertical uplift rate, $v$. Erosion discharges zones of highest topography provoking local vertical isostatic reaction that also controls lateral tectonic inflow below the topography. In this context, erosion works as an upward vertical force applied to the surface. Sediment deposition enhances subsidence in the foredeep basins. Adapted from [43].

### 3.1.4. Initial and boundary conditions

The numerical code allows for direct implementation of various possible collision scenarios. We directly infer the deep lithological and rheological structure from available seismic and gravity profiles, thermal distribution, rock mechanics and kinematics data (Fig. 5A, Tables 1 and 2). In the model (Fig. 5A) the colliding lithospheric plates are composed of different lithological layers, or material phases, characterized by specified physical parameters (Table 2). The lateral boundary conditions are horizontal velocities corresponding to the observed convergence rates. The upper boundary condition is set as free surface (plus surface erosion and sedimentation, Eq. 4), the bottom boundary condition is a pliable Winkler (hydrostatic) basement. The implementation of the free upper boundary condition is an important advantage of this approach, making it possible to model the evolution of surface topography and lithospheric deformation [6]. Table 1 specifies the local data used to constrain the models. Input parameters for the thermo-mechanical modeling are summarized in Table 2.

## 3.2. Modelling results

As shown below, the model explains significant differences for the mode of slab dynamics along the Carpathians, as a direct consequence of along-arc variations in lithospheric configuration and tectonic topography. These differences appear to be largely controlled by lateral variations in crustal structure, topography emplacement and surface processes. To account for differences between various parts of the Carpathians, we have run a set of experiments along two profiles (central–northern and the bend zone of the East Carpathians), in which we basically varied the initial thermal state of the lithosphere and the degree of metamorphism in the lower plate.

### 3.2.1. Central–northern part of East Carpathians

Convergence in the northern EESB sector (Fig. 6) is basically characterized by the convergence of old cratonic continental lithosphere with a high degree of crustal metamorphism, an older thermo-tectonic age and fast uplift/erosion processes.

The model predicts a normal, oceanic-type subduction, where the slab holds its strength and integrity (Fig. 6A). This subduction mode develops because the lower plate, with a 150–200 Ma old thermo-tectonic age, is negatively buoyant and sufficiently rigid to be pulled down, similar to an

Table 1
Constraints on continental collision dynamics for the SE Carpathians (Romania)

| Parameter | 'Typical' collision (EESB) | 'Unusual' collision (MB) |
|---|---|---|
| Crust geometry | Dense low buoyant: thick crust below syn- and post-collisional sediments | Highly buoyant: thin crust below thick syn- and post-collisional sediments |
| Uplift patterns | Uplift and erosion onset during collision (15–12 Ma), 5 km of uplift | Small-scale to zero uplift during collision. Uplift and erosion largely post-date collision (4–0 Ma), 2–3 km of uplift |
| Foredeep geometry | Typical: 3–6 km, wedge-type foredeep | Atypical: symmetrical, up to 10 km syn- and post-collision 'foredeep' |
| Shortening | High internal shortening and low foreland offset of the contact thin-skinned nappe pile | Low internal shortening and high foreland offset of the contact thin-skinned nappe pile |
| Indentation | Stable: Minor post-collisional deformation and sedimentation | Unstable: Major post-collisional deformation and sedimentation with no thrusting connection |

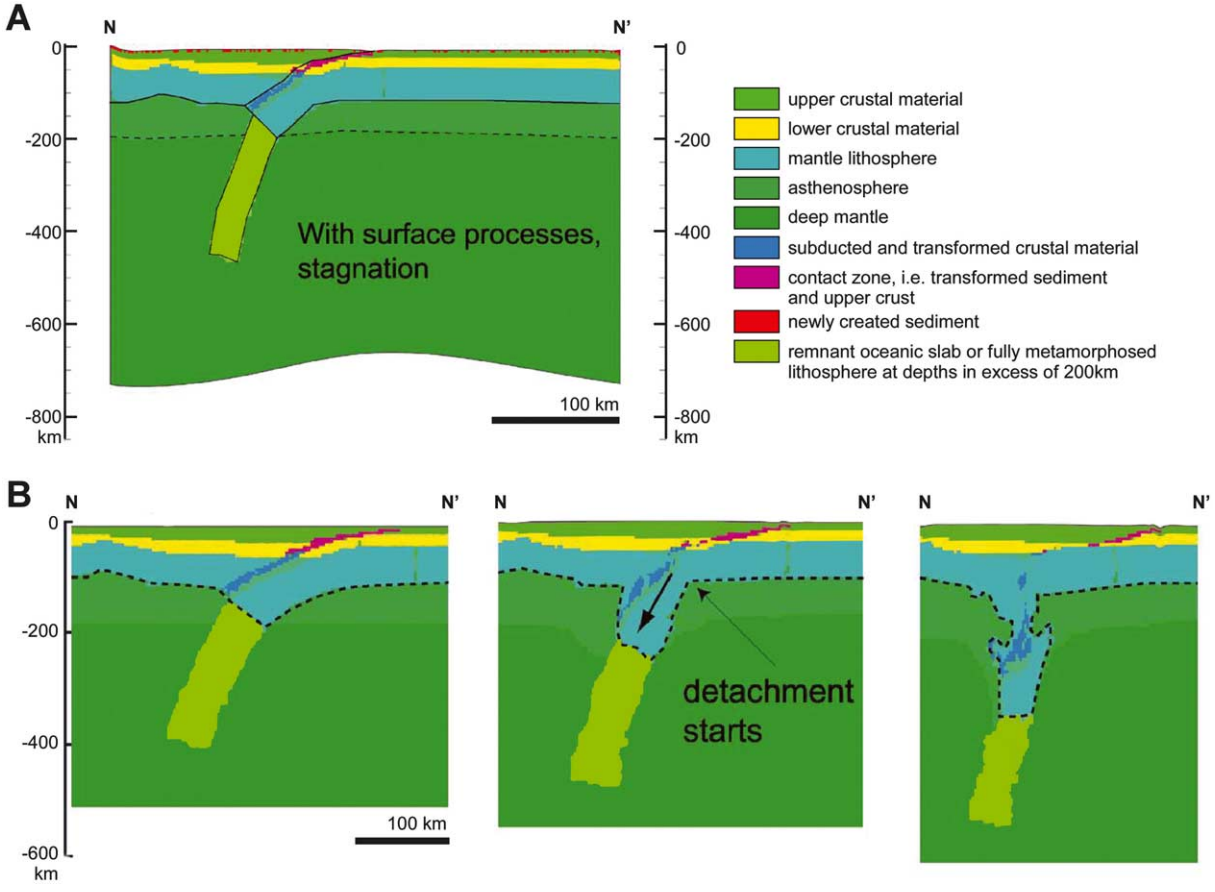


Fig. 6. (A) Modelling results for the central–northern East Carpathians cross-section for scenario with high thermal age (150 Ma), low buoyancy in the subducting plate and active surface processes (see Tables 1 and 2 for details). Note the stable character of subduction: the slab preserves its internal coherence. (B) Three successive steps in the modelling scenario in which detachment occurs mainly due to strain localization caused by flexural stresses at shallow levels (in the absence of fast erosion).

Table 2
Parameters used in modelling experiments

| Parameter | Value |
|---|---|
| Crustal thickness $h_c$ | 40–45 EESB, 35–40 MB [km] |
| Upper crustal thickness | 0.5 $h_c$ |
| Lower crustal thickness | 0.5 $h_c$ |
| Syn- and post-collision sediments | 3–5 EESB, 6–13 MB [km] |
| Convergence rate | 30, 15 on both sides [mm/yr] |
| Thermo-tectonic age, $t_a$ | 150–200 EESB, 15 MB [Ma] |
| Timing onset of uplift | 15–11 EESB, 5–0 MB [Myr] |
| Total erosion estimates | 6 EESB, 5 MB [km] |
| Coefficient of erosion $k$ | 0, 500, 1000 (no, intermediate, rapid) [$m^2$/yr] |
| Background strain rate | variable, $10^{-17}$ to $10^{-13}$ [$s^{-1}$] |
| Young's modulus $E$ | 80 [GPa] |
| Poisson's ratio $v$ | 0.25 |
| Universal gas constant $R$ | 8.314 [J/mol K] |
| Power law constant $A_{c1}$* | $1.26\times10^{-7}$ (wet granite) [$MPa^{-n}$ $s^{-1}$] |
| Power law constant $n_{c1}$ | 2.7 (wet granite) |
| Creep activation energy $H^*_{c1}$ | 134 (wet granite) [kJ $mol^{-1}$] |
| Power law constant $A_{c2}$* | $5.01\times10^{-15}$ (dry diorite) [$Pa^{-n}$ $s^{-1}$] |
| Power law constant $n_{c2}$ | 2.4 (dry diorite) |
| Creep activation energy $H^*_{c2}$ | 212 (dry diorite) [kJ $mol^{-1}$] |
| Power law constant $A_m$* | $7\times10^{-14}$ (olivine) [$Pa^{-n}$ $s^{-1}$] |
| Power law constant $n_m$ | 3 (olivine) |
| Creep activation energy $H^*_m$ | 520 (olivine) [kJ $mol^{-1}$] |
| Density $\rho_s$ | 2300 (uncompacted sediment) [kg $m^{-3}$] |
| Density $\rho_{c1}$ | 2650 (upper crust) [kg $m^{-3}$] |
| Density $\rho_{c2}$ | 2900 (lower crust) [kg $m^{-3}$] |
| Density $\rho_m$ | 3330 (lithospheric mantle) [kg $m^{-3}$] |
| Density $\rho_a$ | 3250 (asthenosphere) [kg $m^{-3}$] |
| Gravity constant $g$ | 9.8 [m $s^{-2}$] |
| Initial lithospheric thickness $a_t$ | 250 (initial geotherms) [km] |
| Temperature at the base of the lithosphere $T_m$ | 1330 (for initial geotherms) [°C] |
| Thermal diffusivity $\chi_{c1}$ | $8.3\times10^{-7}$ (upper crust) [$m^2$ $s^{-1}$] |
| Thermal diffusivity $\chi_{c2}$ | $6.7\times10^{-7}$ (lower crust) [$m^2$ $s^{-1}$] |
| Thermal diffusivity $\chi_m$ | $8.75\times10^{-7}$ (mantle lithosphere) [$m^2$ $s^{-1}$] |
| Thermal conductivity $k_s$ | 1.6 (uncompacted sediment) [W $m^{-1}$ $K^{-1}$] |
| Thermal conductivity $k_{c1}$ | 2.5 (upper crust) [W $m^{-1}$ $K^{-1}$] |
| Thermal conductivity $k_{c2}$ | 2 (lower crust) [W $m^{-1}$ $K^{-1}$] |
| Thermal conductivity $k_m$ | 3.5 (mantle lithosphere) [W $m^{-1}$ $K^{-1}$] |
| Radiogenic decay depth | 10 (upper crust) [km] |
| Surface heat production | $9.5\times10^{-10}$ (upper crust) [W $kg^{-1}$] |

The set of flow law parameters from [44] was chosen to represent rheologies of main constituent rocks of the lithosphere. Other parameters are from [45,46].

oceanic lithosphere subduction scenario. Subduction, with increased shortening of the orogenic wedge, is likely to continue during the collision process. A larger quantity of upper crustal material than normally is involved in subduction, which subsequently is directly translated into increased syn- and post-collisional calc-alkaline volcanism. The latter is constrained by the larger quantity of sediment fluids involved in subduction. As pointed out in Section 3.1, increased erosion of the upper plate inhibits detachment of the lower plate, at least during collision: fast erosion unloads the upper plate, reducing the effective gravity force and favoring stable subduction of the downgoing EESB plate (see also [7]). Eroded sediments are driven away from the East Euro-

pean subduction system and deposited southward, into the Focsani depression, i.e. into the Moesian subduction system [37]. Models involving fast erosion suppress the shallow detachment of the subducted slab in the central–northern East Carpathians (Fig. 6B). The model also predicts a modest amount of crustal thinning in the backarc (Transylvania) basin because of the thermal anomaly generated by the magmatic fluids in ascent.

### 3.2.2. *Bend zone of the East Carpathians*

The numerical experiments on convergence in the East Carpathians bending area correspond to very young thermal age and a decreased role for surface processes during collision. Two end member cases with high and low degrees of crustal metamorphism were investigated. Under conditions of young thermo-tectonic age (hot geotherm), the MB plate cannot be efficiently underthrusted. The plate heats up and remains locally buoyant below the collision zone. At greater depths, the thermally weakened dense part of the mantle lithosphere is surrounded by lighter asthenosphere, becomes unstable, and sinks down due to a developing Raleigh–Taylor (RT) instability. The subduction rate in this case has little to do with the convergence rate: if it is significantly higher than the convergence rate, subduction starts operating in cycles, since the time needed to transport new material to the convergent zone is longer than that globally needed to 'subduct' it. The model predicts that the lower plate crust decouples from the lithosphere and stagnates at lithospheric depths to form a double crustal zone (Fig. 7) that stops the 'oceanic-type' subduction process. The slab is first slowed down at lithospheric depths and then heats up due to heat conduction from the hot asthenosphere. As a result, the plate gradually loses strength and viscosity, and gravitational pull-down starts to stretch the dense part of the mantle lithosphere. A RT instability develops, and the lithosphere continues to elongate with increasing velocity at asthenospheric depths. Portions of the slab may preserve brittle strength sufficient for stress accumulation and subsequent seismicity. Earthquake generation can also occur as a result of plastic instability at high temperature, when runaway shear slip can occur even at low shear stresses [48]. As a result of the subduction process, crustal material reaches the asthenosphere in a too small quantity to generate significant calc-alkaline volcanism. In contrast, the positive thermal anomalies created below the overriding plate favor the formation of alkaline volcanism. These thermal anomalies are also compatible with the mantle convection patterns induced by gravitational sinking of the slab, as predicted by thermal modelling constrained by P-wave tomography in the Vrancea area [48]. The double Moho formation and the buoyancy generated by the crustal underplating favor uplift in the overriding plate in the late post-collisional stages. At the same time, the locked system dragged down by the heavy hanging slab leads to major subsidence, mostly localized in the lower plate. Overall, the thermal age (reflected in the geotherm) effect is more important than the degree of crustal metamorphism (see [6]) for the development of RT instabilities.

## 4. Implications for interaction between lithospheric and surface processes in the Carpathians system

Results of modelling presented above fit the first-order geometrical, geological and geophysical features of the East Carpathians. The model is consistent with the lateral variations in orogenic shortening in the orogenic belt, uplift and subsidence patterns during syn- and post-collision phases and present-day upper mantle structure and dynamics. It explains the character and zonation of the seismicity observed in the Vrancea area. The model also yields insights into the type and characteristics of the Neogene volcanism. In addition, it supports the assumption that subduction and collision processes are influenced by inherited rheology and lithospheric memory of the lower plate(s).

The unusual character of the subduction along the Carpathians arc appears to be primarily controlled by the thermo-tectonic age of the underthrusted lithosphere and lateral variations in the interplay between the lithosphere and surface processes.

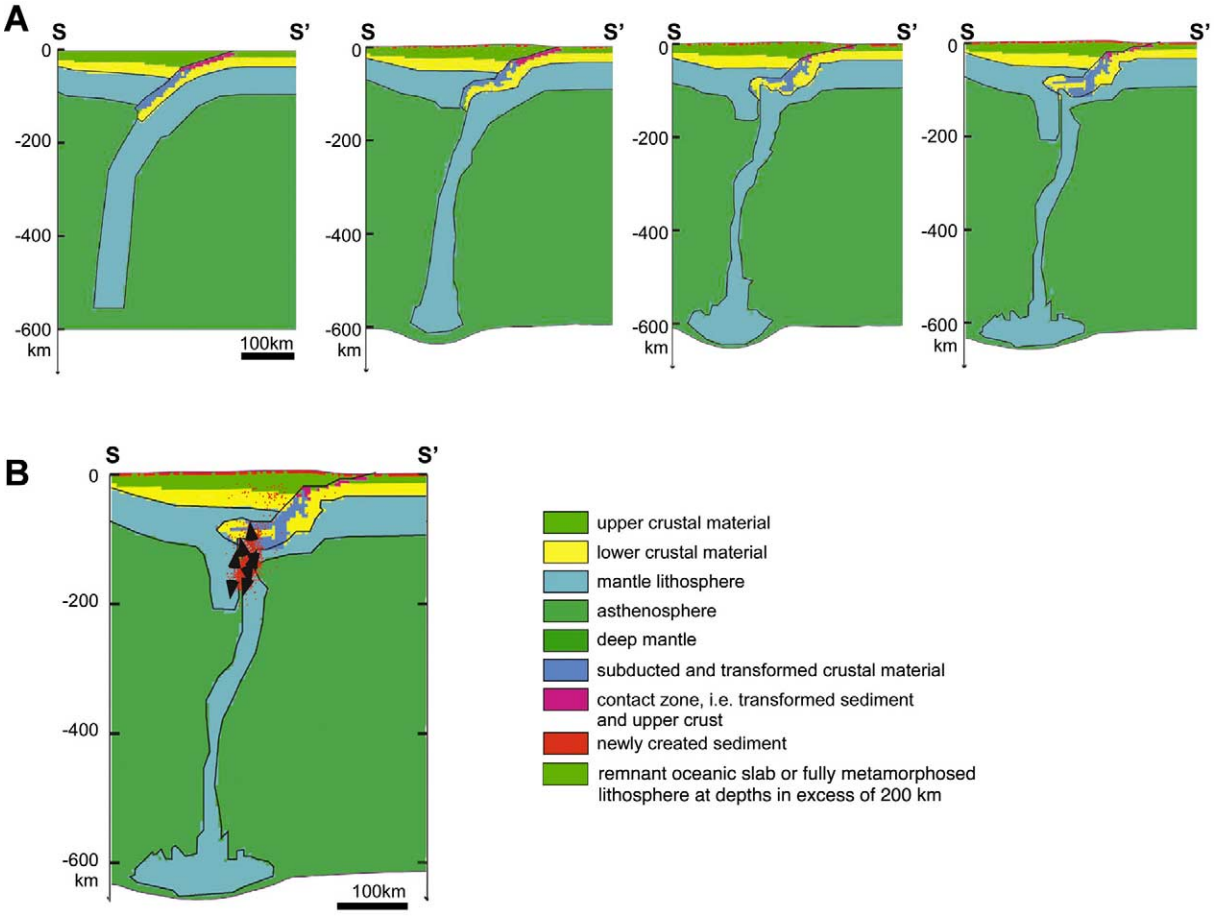


Fig. 7. (A) Modelling results for the cross-section located in the bend zone of the East Carpathians. Four successive steps for a scenario with young thermal age, high buoyancy of the lower plate (due to a low degree of metamorphism) and no surface processes. Note the unstable character of subduction: the slab loses the coherence due to internal heat-up. This results in development of a RT instability, acceleration of sinking to great depths due to gravity stretching, strength depth zonation and the formation of double subvertical high-velocity bodies down to 200 km depths. (B) Case with a low degree of metamorphism (high buoyancy of the lower plate) and small thermo-tectonic age (Tables 1 and 2). A double Moho forms and model predictions closely fit the tomography data for the Vrancea area. Depth strength zonation is compared with the vertical clustering of Vrancea earthquakes (black arrows show mostly vertical stretching focal mechanisms). Other conventions as in Fig. 6.

### 4.1. Volcanism

The thermal structure and the amount of upper crustal material involved in subduction inferred from the thermo-mechanical model is consistent with the documented bi-modal character of the Neogene volcanism in the East Carpathians (Fig. 3B).

Massive calc-alkaline stratovolcanism took place in the plate overriding EESB (i.e. central–northern segment) in the 'typical' subduction domain (Fig. 3B). This is a direct result of the large quantity of crustal material introduced into the asthenosphere during the collision. The volcanism has a medium-K to high-K calc-alkaline to shoshonitic composition, with older Miocene to Early Pliocene ages (main period 12–6 Ma) (e.g. [36]) and a significant migration towards the south through time. The isotopic composition shows high crustal contamination [49]. Variations in volcanic ages from NW to SE along the chain may be related to along-arc variations in crustal struc-

tures (i.e. thicker basement and lower crustal material towards the central part of the East Carpathians).

In contrast, in the upper plate zone that overrides the MB in the bending area, the volcanism is mafic alkaline, with young, Pliocene to Quaternary ages (up to 0.2 Ma), and a strong asthenosphere (oceanic island basalt-type mantle source) component [50]. In this area the isotopic characteristics are derived from a mantle which was affected by earlier subduction (e.g. [50]) (Fig. 3B). This means that the volcanism is related more to the thermal anomaly developed below the overriding plate than to upper crust heated up in the asthenosphere. This volcanism is also typical for late stages of collision, when alkaline-type magmas develop in relationship with post-collisional stress relaxation structures.

In the upper plate area, at the transition between the two types of subduction (i.e. Harghita Mts.), the volcanism is transitional between the calc-alkaline and alkaline types (Fig. 3B).

### 4.2. *Shortening in the orogenic belt, syn- and post-collision vertical motions and basin development*

The thermo-tectonic model predicts the complex patterns of vertical movements recorded in the aftermath of collision in the Moesian–Carpathians bending domain (Fig. 3A). The subduction system became detached and blocked in the early phases and failed to induce significant shortening and associated uplift during collision: only a small amount of internal shortening is observed in the thin-skinned thrust belt (e.g. [18]) associated with insufficient uplift to induce significant erosion (in any case below FT resolution, see [1]). In contrast, the continuation of oceanic-type subduction in the central–northern domain means that a large part of the former passive margin, comprising thinned to stable continental crust of the lower plate, was underthrusted in the collision process. This induced significant internal shortening in the thin-skinned nappe pile at the contact [18], 4–5 km of uplift followed by erosion [1] and the basement exhumation observed in the northern Bucovinic system (sensu [27]). During the post-collisional phase, in this central–northern part, the system became welded. The minor uplift observed is related to continuation of the main convergence phase. In contrast, the post-collisional phase of the bending area is characterized by large subsidence in the foredeep, which can be explained as a result of drag of the vertical stretching slab (Fig. 3A). A large amount of uplift is recorded towards the neighboring western nappe pile, with no orogenic-related shortening. The pull of the vertical stretching slab accounts for a reduction in the orogenic load needed for the observed deflection in the foreland, as observed also by recent 3D flexural modelling [51].

In addition to the effect of the vertical sinking slab, the evolution of the Focsani basin appears to be affected by a succession of other coevally operating tectonic processes. Quantitative modelling has documented the key role of pre-orogenic Middle Miocene (14 Ma) extension (coeval with the late stages in the opening of the adjacent Black Sea basin), in the generation of accommodation space for the deposition of 13 km Miocene to Recent sediments [15]. This pre-orogenic extension has led to decoupling of the crust and mantle lithosphere, promoting Pliocene–Quaternary crustal-scale folding with a characteristic wavelength of 80 km, compatible with the predictions from thermo-mechanical folding models [5,25].

As pointed out above, the Trotus fault is a lithospheric-scale structure separating two major domains (Fig. 3A). Its complex kinematics records the direct interaction between the northern lower plate domain, involved in underplating, and the locked southern sector. As a result, sinistral movement was induced [15,18] during collision and apparently still takes place [52]. Subsidence of the locked southern domain during post-collision may have induced the downward throw of this fault to the south.

The predicted crustal thinning in the adjacent backarc basin is compatible with the observed 4–5 km Miocene subsidence in the Transylvania basin [53], a distinct feature of which is the absence of associated normal faults. This explains to a large extent the pronounced differences in elevation, structure and thermal history between the Pannonian Basin, characterized by high heat flow, large

stretching factors and low topography [8] and the Transylvania Basin, characterized by low heat flow, absence of stretching and high elevation. Differential far-field stresses between the central–northern and the southern East Carpathians collision zones enhanced the first (Late Miocene) inversion in the northern Pannonian basin (see also [5,26]) and accelerated the uplift of the northern Transylvania basin. Lateral variations in the Carpathians lower plate behavior during subduction provide further constraints on the geometry and kinematics of the entire Carpathians chain during syn- and post-collisional times. Intensified collision with the mechanically strong East European/Scythian lithosphere between the Polish Trough and the Trotus fault induced a linear geometry of the orogen in this particular fold belt segment.

### 4.3. *Upper mantle structure and dynamics of vertical motions at the surface*

Our model is consistent with the presence of the high-velocity bodies depicted by seismic tomography studies (Fig. 2) south of the Trotus fault (e.g. [10]). Detachment and RT instability resulting from the highly buoyant crust and reduced rates of collision leads to a thermal resettlement and slab melting. This process caused the thinned high-density distal parts of MB to gravitationally sink into the asthenosphere with increasing velocity with depth. The differences in velocity are accommodated through vertical stretching of the slab, flowing towards already thinned areas characterized by a higher degree of thermal re-equilibration. Failure generates earthquakes in zones of the slab retaining some strength: the modelled zonation of these areas is in agreement with the observed depth zonation. Slab thickness variations in depth are supported by recent results from high-resolution tomographic studies [20].

The upper plate also starts to detach, as a large part of the mantle joins the vertical descent, possibly down to 200 km. These processes presently induce active topography formation and neotectonic processes. At the site of the sinking slab active subsidence takes place in the Focsani basin. The evolution of this subsidence [2,15] is in good agreement with the modelled section, as subsidence accelerated from Pliocene towards maximum values in the Quaternary (Fig. 4B).

Detachment of the upper plate in the neighboring sector induced a strong rebound of the upper plate, and this is in good agreement with the accelerated uplift, tilted geometry and high topography/active geomorphology of Lower to Middle Quaternary sediments on the western flank of the Focsani basin. The middle-scale uplift of the eastern flank of the Focsani basin relates to foreland bulge uplift, due to increasing dip through time of the slab. In this respect, the active neotectonic Peceneaga–Camena fault zone represents normal faulting on the upper part of the lower plate in the maximum curvature zone, being favored by the strong mechanical contrast along this zone between MB and North Dobrogea orogen (e.g. [24]) (Fig. 8). This complex pattern of vertical movements is in good agreement with surface transport models based on present-day sediment river loads and prediction of the areal distribution of erosion and deposition (e.g. [26,54]). The predicted geometry at lithospheric levels does not require lateral migration in time of slab mechanisms, as assumed by previous models (e.g. [9,12,13]), is in good agreement with the absence of depocenter migration in this sector of the SE Carpathians foreland (Fig. 4B,C), and assumes a coherent mechanism of slab evolution in the entire sector of the MB. Atypical kinematics, associated with the MB end member mode of subduction, also occurs further westwards, in the South Carpathians foredeep domain and its westward Dinaridic/Balkans connection. Here, similar to the Focsani basin, up to 2–3 km of foredeep subsidence took place, post-dating the Upper Miocene collision moment [33]. Blocking the subduction system in the bend zone in the early phases of collision promotes subsequent build-up of intraplate stresses in the entire Moesian domain, promoting lithospheric buckling (sensu [35]). The latter is suggested by lithosphere heat-up inducing crust/mantle decoupling.

In the EESB, seismic tomography (e.g. [10]) cannot conclusively identify a high-velocity slab, or whether the image displays the usual thick, stable and cold European lithosphere. The high-

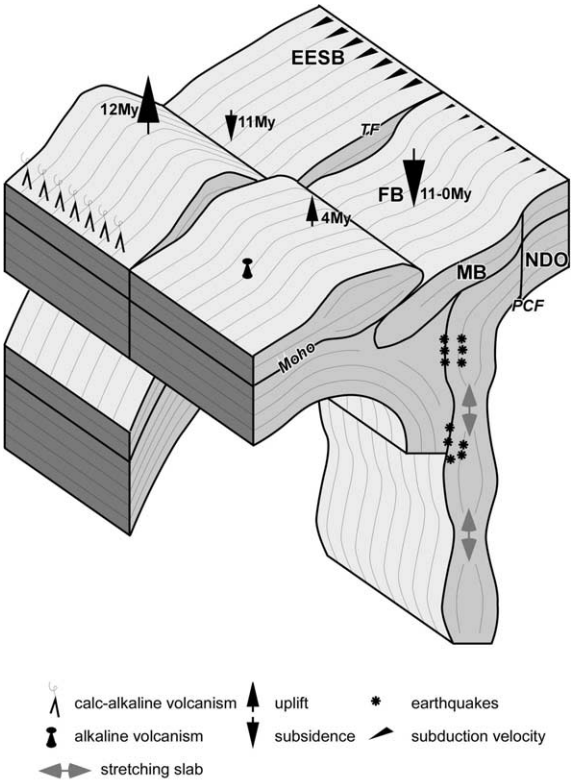


Fig. 8. 3D cartoon of spatial variations in mode of subduction along the East Carpathians orogen and their expression in spatial and temporal varying patterns of seismicity, volcanism and vertical motions. EESB: East-European/Scythian block; MB: Moesian block; NDO: North Dobrogea orogen; TF: Trotus fault; PCF: Peceneaga–Camena fault; FB: Focsani Basin.

velocity sub-horizontal body positioned at the depth of 400–600 km under the Pannonian basin cannot be directly correlated to the EESB eastward of the Romanian Carpathians. The modelling presented in this paper suggests that with increased surface process activity during collision and taking into the account the low-buoyant lower plate block, the strength coherence of the slab will be maintained during the post-collisional period, counteracting slab detachment. However, the short time interval of the collisional processes (3–4 Ma) suggests that the present-day 11 Ma steady state is a subduction-locked system, without major tectonic processes. As a result, the present-day topography reflects only the late-stage collisional rebound, with a minor role for neotectonic processes and associated kinematics.

### 4.4. Stretching slab and seismicity in the Vrancea area

The focal mechanism solutions are not straightforward for the intermediate-depth Vrancea seismic body. The intermediate-depth destructive events (e.g. 1940, 7.7 $M_w$; 1977, 7.4 $M_w$; 1986, 7.1 $M_w$; 1990, 6.9 $M_w$) show mainly NW–SE-oriented compression (e.g. [16]). However, other smaller intermediate-depth events show NE–SW-oriented compression (e.g. [16]) and an apparent zonation with depth. The results of our modelling shed light on this bi-modal character: some of the Vrancea earthquakes (bend zone, MB, Fig. 2) appear to be generated by contact between the slab in accelerated descent and the detached mantle of the upper plate down to 200 km. Part of the seismicity and the cylindrical geometry of the Vrancea body could also be generated by failure inside the lower plate due to its vertical stretching. Therefore, the compression directions in the Vrancea seismogenic body are not related to mechanical plate interaction only. The tension direction of all studied focal mechanisms is vertical to subvertical, demonstrating stretching of the slab and its gravitational sinking into the asthenosphere (Fig. 8). In contrast, seismicity in the subduction zone of the distal parts of the EESB is minor, and mostly relates to smaller-scale crustal events.

## 5. Conclusions

This modelling study demonstrates that in low-rate convergence regimes such as the Carpathians, the subducted lithosphere has enough time to interact with the mantle to advance towards a thermal resettlement. A particularly novel feature of our modelling is the incorporation of lateral variations in the thermo-mechanical structure of the subducted lithosphere along the strike of the orogen. Lithospheric configuration of the underthrusted lithosphere and tectonic topography appears to be a prime factor in slab behavior in the

aftermath of continental collision. The unusual character of the subduction along the Carpathians arc appears to be primarily controlled by the thermo-mechanical age of the underthrusted lithosphere and lateral variations in the interplay between the lithosphere and surface processes. The results of thermo-tectonic modelling performed on the post-collisional East Carpathians are in striking agreement with first-order patterns of geometrical, geological and geophysical observations in the area. Particularly interesting in this respect are the observed vertical motions and foredeep basin development, upper mantle structure and seismicity in the Vrancea area. The model explains for the first time in a consistent way the occurrence of a very deep, unusual foredeep basin geometry and anomalous subsidence in front of the bend zone of the Carpathians. It accounts for the source–sink relationships between coevally uplifting Carpathians and rapidly subsiding foredeep basins as consequences of the lack of continuing orogenic shortening. An effective top-down control on collision dynamics is suggested, pointing to a more limited role for bottom-up effects of slab break-off on surface processes in the terminal collisional phase in this area.

## Acknowledgements

This work was funded through research grants from the Netherlands Centre for Integrated Solid Earth Sciences and by INSU-CNRS IT program (E.B.). C. Dinu, F. Horvath, M. Tarapoanca, G. Bada and H. Doust are thanked for stimulating discussions. Y. Podladchikov and A. Poliakov are thanked for sharing the Parovoz code with us. Constructive, critical reviews and suggestions by C. Hall and J.P. Burg and editorial comments by S.D. King are acknowledged. ***[SK]***

## References

[1] C. Sanders, P. Andriessen, S. Cloetingh, Life cycle of the East Carpathian Orogen: erosion history of a doubly vergent critical wedge assessed by fission track thermochronology, J. Geophys. Res. 104 (1999) 29,095–29,112.

[2] L. Matenco, G. Bertotti, S. Cloetingh, C. Dinu, Subsidence analysis and tectonic evolution of the external Carpathian-Moesian platform region during Tertiary times, Sediment. Geol. 156 (2003) 71–94.

[3] L. Matenco, R. Zoetemeijer, S. Cloetingh, C. Dinu, Lateral variations in mechanical properties of the Romanian external Carpathians: inferences of flexure and gravity modelling, Tectonophysics 282 (1997) 147–166.

[4] R. Zoetemeijer, C. Tomek, S. Cloetingh, Flexural expression of European continental lithosphere under the western outer Carpathians, Tectonics 18 (1999) 843–861.

[5] F. Horváth, S. Cloetingh, Stress-induced late-stage subsidence anomalies in the Pannonian basin, Tectonophysics 266 (1996) 287–300.

[6] E.B. Burov, L. Jolivet, L. LePourhiet, A. Poliakov, A thermomechanical model of exhumation of high pressure (HP) and ultra-high pressure (UHP) metamorphic rocks in alpine-type collision belts, Tectonophysics 342 (2001) 113–136.

[7] G. Toussaint, E. Burov, L. Jolivet, Modelling collision of young continental plates: unstable versus stable slab dynamics, Geology (2003) in press.

[8] D. Ioane, L. Atanasiu, Gravimetric geoids and geophysical significances in Romania, in: D. Ioane (Ed.), Monograph of Southern Carpathians, Reports on Geodesy 7, Institute of Geodesy and Geodetic Astronomy, Warsaw University of Technology, Warsaw, 1998, pp. 157–175.

[9] F. Wenzel, U. Achauer, D. Enescu, E. Kissling, R. Russo, V. Mocanu, G. Musacchio, Detailed look at final stage of plate break-off is target study in Romania, EOS 79 (1998) 590–594.

[10] M.J.R. Wortel, W. Spakman, Subduction and slab detachment in the Mediteranean-Carpathian region, Science 290 (2000) 1910–1917.

[11] F. Radulescu, Seismic models of the crustal structure in Romania, Rev. Roum. Géol. Géophys. Géogr. Sér. Géophys. 32 (1988) 13–17.

[12] B. Sperner, F. Lorenz, K. Bonjer, S. Hettel, B. Muller, F. Wenzel, Slab break-off – abrupt cut or gradual detachment? New insights from the Vrancea Region (SE Carpathians, Romania), Terra Nova 13 (2001) 172–179.

[13] Z. Gvirtzman, Partial detachment of a lithospheric root under the southeast Carpathians: Toward a better definition of the detachment concept, Geology 30 (2002) 51–54.

[14] F. Horvath, Towards a mechanical model for the formation of the Pannonian basin, Tectonophysics 225 (1993) 333–357.

[15] M. Tarapoanca, G. Bertotti, L. Matenco, C. Dinu, S. Cloetingh, Architecture of the Focsani depression: A 13 km deep basin in the Carpathians bend zone (Romania), Tectonics (2003) in press.

[16] M.C. Oncescu, K.P. Bonjer, A note on the depth recurrence and strain release of large Vrancea earthquakes, Tectonophysics 272 (1997) 291–302.

[17] H.-G. Linzer, W. Frisch, P. Zweigel, R. Girbacea, H.-P. Hann, F. Moser, Kinematic evolution of the Romanian Carpathians, Tectonophysics 297 (1998) 133–156.

[18] L. Matenco, G. Bertotti, Tertiary tectonic evolution of the external East Carpathians (Romania), Tectonophysics 316 (2000) 255–286.
[19] R.A. Stephenson, V.I. Mocanu, I. Panea, L. Matenco, C.C. Diaconescu, the DACIA-PLAN team, Deep seismic reflection line across the southeastern Carpathian belt (Vrancea Zone) and its foreland basin, Geophys. Res. Abstr. 4 (2002) 253.
[20] M. Martin, CALIXTO working group, High resolution seismic P-wave tomography for SE-Romania, in: European Geophysical Society 2003, Nice, France, Geophys. Res. Abstr. 5 (2003) 10512.
[21] H. Bijwaard, W. Spakman, E.R. Engdahl, Closing the gap between regional and global travel time tomography, J. Geophys. Res. 103 (1998) 30–55.
[22] S. Cloetingh, E.B. Burov, Thermomechanical structure of European continental lithosphere; constraints from rheological profiles and EET estimates, Geophys. J. Int. 124 (1996) 695–723.
[23] M. Andreescu, C. Demetrescu, Rheological implications of the thermal structure of the lithosphere in the convergence zone of the Eastern Carpathians, J. Geodyn. 31 (2001) 373–391.
[24] A. Lankreijer, V. Mocanu, S. Cloetingh, Lateral variations in lithosphere strength in the Romanian Carpathians: Constraints on basin evolution, Tectonophysics 272 (1997) 269–290.
[25] S. Cloetingh, F. Horváth, G. Bada, A. Lankreijer (Eds.), Neotectonics and Surface Processes: The Pannonian Basin and Alpine/Carpathian System, EGU Spec. Publ. (2002) 295 pp.
[26] S. Cloetingh, F. Horváth, R.A. Stephenson, G. Bertotti, G. Bada, L. Matenco, TecTop working group, Probing tectonic topography at the aftermath of continental convergence in the Pannonian-Carpathian system, EOS 84 (2003) 89–96.
[27] M. Sandulescu, Cenozoic Tectonic History of the Carpathians, in: L.H. Royden, F. Horvath (Eds.), The Pannonian Basin, A Study in Basin Evolution, AAPG Mem. 45 (1988) 17–25.
[28] B.C. Burchfiel, Geology of Romania, Geological Society of America, 1976, 82 pp.
[29] L.H. Royden, The tectonic expression of slab pull at continental convergent boundaries, Tectonics 12 (1993) 303–325.
[30] L. Csontos, Tertiary tectonic evolution of the Intra-Carpathian area: a review, Acta Vulcanol. 7 (1995) 1–13.
[31] S.M. Schmid, T. Berza, V. Diaconescu, N. Froitzheim, B. Fuegenschuh, Orogen-parallel extension in the South Carpathians during the Paleogene, Tectonophysics 297 (1998) 209–228.
[32] L. Matenco, S. Schmid, Exhumation of the Danubian nappes system (South Carpathians) during the early Tertiary: inferences from kinematic and paleostress analysis at the Getic/Danubian nappes contact, Tectonophysics 314 (1999) 401–422.
[33] G. Bertotti, L. Matenco, S. Cloetingh, Vertical movements in and around the SE Carpathian foredeep: Lithospheric memory and stress field control, Terra Nova 15 (2003) 299–305.
[34] D. Enescu, D. Danchiv, A. Bala, Lithosphere structure in Romania II. Thickness of Earth crust. Depth-dependent propagation velocity curves for P and S waves, Stud. Cercet. Geol. Geofiz. Geogr. Ser. Geofiz. 30 (1992) 3–19.
[35] S. Cloetingh, E. Burov, A. Poliakov, Lithosphere folding: Primary response to compression? (from central Asia to Paris basin), Tectonics 18 (1999) 1064–1083.
[36] Z. Pecskay, J. Lexa, A. Szakacs, K. Balogh, I. Seghedi, V. Konecny, M. Kovacs, M. Marton, M. Kaliciak, V. Szeky-Fux, T. Poka, P. Gyarmaty, O. Edelstein, E. Rosu, B. Zec, Space and time distribution of Neogene-Quaternary volcanism in the Carpatho-Pannonian region, Acta Volcanol. 7 (1995) 15–29.
[37] D. Jipa, Late Neogene-Quaternary evolution of Dacian basin (Romania). An analysis of sediment thickness pattern, Geo-Eco-Marina 2 (1997) 128–134.
[38] M. Radoane, N. Radoane, D. Dumitriu, Geomorphological evolution of longitudinal river profiles in the Carpathians, Geomorphology 50 (2003) 293–306.
[39] A.N.B. Poliakov, Y. Podladchikov, C. Talbot, Initiation of salt diapirs with frictional overburden: numerical experiments, Tectonophysics 228 (1993) 199–210.
[40] P.A. Cundall, Numerical experiments on localization in frictional materials, Ing. Arch. 59 (1989) 148–159.
[41] F. Sobouti, J. Arkani-Hamed, Thermo-mechanical modelling of subduction of continental lithosphere, Phys. Earth Planet. Inter. 131 (2002) 185–203.
[42] R. Hassani, J. Chery, Control of extensional tectonics by crustal rheology numerical experiments, Geology 24 (1996) 1095–1098.
[43] J.P. Avouac, E.B. Burov, Erosion as a driving mechanism of intracontinental mountain growth, J. Geophys. Res. 110 (1996) 17747–17769.
[44] S.H. Kirby, A.K. Kronenberg, Rheology of the lithosphere: selected topics, Rev. Geophys. Space Phys. 25 (1987) 1219–1244.
[45] D. Turcotte, G. Schubert, Geodynamics: Applications of Continuum Physics to Geological Problems, Wiley, New York, 1982, 450 pp.
[46] B. Parsons, J.G. Sclater, An analysis of the variation of ocean floor bathymetry and heat flow with age, J. Geophys. Res. 32 (1977) 803–827.
[47] E.B. Burov, M. Diament, The effective elastic thickness (Te) of continental lithosphere; what does it really mean?, J. Geophys. Res. 100 (1995) 3905–3927.
[48] A. Ismail-Zadeh, B. Mueller, G. Schubert, Three-dimensional numerical modeling of contemporary mantle flow and tectonic stress beneath the earthquake-prone southeastern Carpathians, Phys. Earth Planet. Inter. (2003) in press.
[49] P.R.D. Mason, I. Seghedi, A. Szakacs, H. Downes, Magmatic constraints on geodynamic models of subduction in the East Carpathians, Romania, Tectonophysics 297 (1998) 157–176.

[50] I. Seghedi, I. Balintoni, A. Szakacz, Interplay of tectonics and neogene post-collisional magmatism in the intracarpathian region, Lithos 45 (1998) 483–497.
[51] M. Tarapoanca, D. Garcia-Castellanos, G. Bertotti, L. Matenco, S. Cloetingh, Role of the 3D distributions of load and lithospheric strength in arcuate orogenic arcs: poly-stage subsidence in the Carpathians foredeep, Earth Planet. Sci. Lett., submitted.
[52] A.G.A. van der Hoeven, B.A.C. Ambrosius, V. Mocanu, W. Spakman, Crustal motions in the Eastern Carpathians (Vrancea), measured by GPS, Geophys. Res. Abstr. 5 (2003) 3918.
[53] D. Ciulavu, C. Dinu, S. Cloetingh, Late Cenozoic tectonic evolution of the Transylvania basin and northeastern part of the Pannonian basin: Constraints from seismic profiling and numerical modelling, in: S. Cloetingh, F. Horvath, G. Bada, A. Lankreijer (Eds.), Neotectonics and Surface Processes: The Pannonian Basin and Alpine/Carpathian System, EGU Spec. Publ. 3 (2002) 105–120.
[54] D. Garcia-Castellanos, Interplay between lithospheric flexure and river transport in foreland basins, Basin Res. 14 (2002) 89–104.